Iranica Journal of Energy & Environment 4 {(3) Geo-hazards and Civil Engineering)}: 239-246, 2013
ISSN 2079-2115
IJEE an Official Peer Reviewed Journal of Babol Noshirvani University of Technology
DOI: 10.5829/idosi.ijee.2013.04.03.10

BUT

Shape Optimization of Hollow Concrete Blocks Using the Lattice Discrete Particle Model

Fatemeh Javidan, Mohammad Safarnejad and Sharif Shahbeyk

Faculty of Civil and Environmental Engineering, Tarbiat Modares University, Tehran, Iran

(Received: January 2, 2013; Accepted in Revised Form: April 30, 2013)

Abstract: Hollow concrete blocks are one of the widely used building elements of masonry structures in which they are normally loaded under combined action of shear and compression. Accordingly and due to their structural importance, the present study intends to numerically search for an optimum shape of such blocks. The optimality index is selected to be the ratio of block's failure strength to its weight, a non-dimensional parameter, which needs to be maximized. The nonlinear analysis has been done using a homemade code written based on the recently developed Lattice Discrete Particle Model (LDPM) for the meso-scale simulation of concrete. This numerical approach accounts for the different aspects of concrete's complex behavior such as tensile fracturing, cohesive and frictional shearing and also its nonlinear compressive response. The model parameters were calibrated against previously reported experimental data. Various two-core configurations for the hollow blocks are examined, compared and discussed.

Key word: Hollow concrete block · Strength · Failure mechanism · Lattice particle discrete method

INTRODUCTION

Due to their light weight, ease of use and reasonable compressive performance, hollow concrete blocks are widely used in masonry structures. Hence, its geometrical design and mechanical properties are of significant importance. Accordingly, many experimental and numerical researches have been conducted in order to obtain logical relations between the structural characteristics of the blocks and their assemblages [1-3]. More complicated works examined the effect of mortar properties and their interface with the blocks [4,5]. The responses of hollow concrete blocks under various loading conditions including concentric and eccentric compression [6,7], flexure [8] and shear [9] have been also empirically assessed.

Alongside with experimental researches, several efforts have been made so far in order to model numerically the complex behavior of blocks, mortar and interface joints. One of the main targets of these studies is to link the global behavior of walls and panels to the properties of individual units and mortar. The most widely-used numerical approaches is found to be the three dimensional finite element (FE) method [10,11]. Utilizing damage models for the constitutive material, [12-14] leaded to acceptable estimation of failure mechanisms of hollow masonry. Lu et al. [15] have used a nonlinear FE model to analyze slender unreinforced masonry hollow walls under eccentric vertical loads focusing on the cavity depth of the blocks. With the purpose of having shape simplicity and ease of manufacture, interlocking mortarless hollow block masonry systems have been developed [16,17]. Compressive strength correlation between the individual block, prism and basic wall panel for this new type of load bearing interlocking blocks has been first obtained both experimentally and numerically [18,19]. A few studies have been also carried out on these structural units emphasizing on various loading conditions and effective geometrical features. Del Coz Díaz et al. [20] have numerically developed a new type of hollow block and optimized its compressive behavior, weight and handling characteristics.

In this research, the lattice discrete particle model (LDPM) as a powerful numerical tool for the simulation of concrete has been employed. This approach let account

Corresponding Author: Sharif Shahbeyk, Faculty of Civil and Environmental Engineering, Tarbiat Modares University, Tehran, Iran Fax: +982182884914, E-mail: *shahbeyk@modares.ac.ir*

for the different aspects of concrete nonlinear behavior such as tensile fracturing, cohesive and frictional shearing and also its nonlinear compressive response. The model is calibrated and validated against available test data. At first, a typical two-hole concrete block was analyzed. Combined compressive-shear loads of various ratios are applied. An optimality index is defined as the ratio of resisted load to block weight. With the aim of increasing the optimality index, three more samples were created by adding horizontal diaphragm or rearranging the holes. Finally, the blocks were compared from both optimality index and failure mechanism points of view.

Lattice Discrete Particle Model

Concrete Meso-structure Modelling: The LDPM is a recently developed method for simulating the failure behavior of discontinuous and heterogeneous materials, such as concrete. The backbone of the current LDPM is the innovative meso-scale approach known as the Confinement Shear Lattice (CSL) Model introduced in literatures [21- 23] and further improved [24]. The Lattice Discrete Particle Model [25,26] combined CSL model with the properties of Discrete Particle Models (DPM). In the LDPM, aggregate content is identified using the mix design and other input properties such as the cement content, aggregate content per unit volume and the grading curve. Next, the aggregates of various sizes are randomly distributed inside the specimen, which helps avoid a bias fracture propagation pattern in the concrete (Fig. 1a). Next, a three dimensional lattice structure tessellates the volume and connects the centers of the adjacent particles resulting in a tetrahedron mesh (Fig. 1b). The connection between each aggregate is called a strut. The constitutive laws of the model are formulated on a finite number of points, called the computational points located between two neighboring aggregates.

Solution Procedure: The basic equation of motion in its matrix form is

$$M\ddot{Q}+C\dot{Q}+P(Q)=F(t) \tag{1}$$

Here, M is the mass matrix, P is the vector of internal forces, C is the damping matrix (which is neglected here), F is the given external load history and Q is the vector of kinematic variables including the translations and rotations. The equation is solved by the explicit method using the central difference approximation in each of the aggregate centers [23]. During the solution process, the

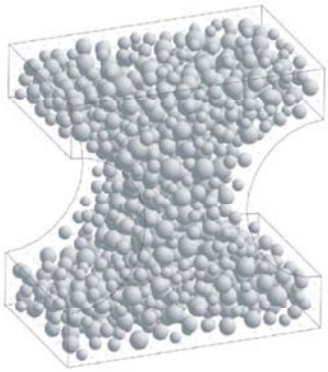

(a)

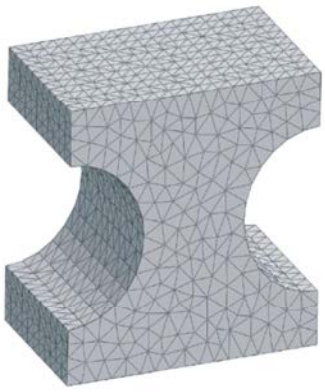

(b)

Fig. 1: (a) Random aggregate distribution and (b) three dimensional tetrahedron mesh of a typical dogbone specimen (Mencarelli [26])

numerical stability condition is reserved by keeping the time step below the permitted limit [23]. Solving the mentioned equation, the displacement field corresponding to the six degrees of freedom for each aggregate center node is determined. Assuming a rigid connection between nodes and computational points, the displacement jumps of the computational points will be obtained as stated in Eq. (2).

$$\left[u(x)\right]=u_I+\theta_I\times(x-x_I)=A_I(x)Q_I \tag{2}$$

In which A is a matrix presented in Eq. (3) and x, u and θ are the coordinates, displacement and rotation matrices of each computation point (I), respectively.

$$A_I(x)=\begin{bmatrix}1&0&0&0&z-z_1&y_1-y\\0&1&0&z_1-z&0&x-x_1\\0&0&1&y-y_1&x_1-x&0\end{bmatrix} \tag{3}$$

Constitutive Relations: The quantities of displacement jumps can then be converted to the required strains at the computational points.

$$\begin{aligned}
&\square_N = n^T[u]/1 = B_{N2}Q_2 - B_{N1}Q_1 \\
&\square_M = M^T[u]/1 = B_{M2}Q_2 - B_{M1}Q_1 \\
&\square_L = n^T[u]/1 = B_{N2}Q_2 - B_{N1}Q_1 \\
&\square_{Ni} = (1/l)n^T A_i(x),\ B_{Li} = (1/l)l^T A_i(x), \\
&B_{Mi} = (1/l)m^T A_i(x),
\end{aligned} \tag{4}$$

Where $\square_N$ is the normal strain and $\square_L$ and $\square_M$ are the tangential strains. Where n is the unit vector directed along the strut and l and m are the two mutually perpendicular tangential unit normal. Also, l is the length of the strut. Combining these normal and tangential strains, the following important stain measures can be introduced.

$$\square = \sqrt{\square_N^2 + \alpha\left(\square_M^2 + \square_L^2\right)} = \sqrt{\square_N^2 + \alpha\square_T^2} \tag{5}$$

Where $\square$ and ω are called the effective and coupling strains, respectively. The term $\square_T$ is the total shear strain. where α is a material property used to control the elastic Poisson's ratio. The constitutive relation of the model is based on the following elastic boundary.

$$s_b(\square,\omega) = \sigma_0(\omega)\exp\left\{\frac{K(\omega)}{s_0}\left\langle \square - \frac{s_0(\omega)}{E}\right\rangle\right\} \tag{6}$$

Where μ is the mesoscale elastic modulus. Also, $K(\omega)$ defines the hardening-softening rates for the different loading paths. where $\sigma_0(\omega)$ is the initial effective strength function and is defined as below:

$$\begin{aligned}
&s_0(\omega) = \begin{cases} s_{01}(\omega) & \omega \le \omega_0 \\ s_{02}(\omega) & \omega > \omega_0 \end{cases} \\
&s_1(?) = \frac{\sigma_c}{\sqrt{(\sin\omega)^2 + \alpha(\cos\omega)^2}} \\
&s_2 = \frac{-(\sigma_t+\sigma_\varepsilon)\sin\omega + \sqrt{\left[(\sigma_t+\sigma_\varepsilon)\sin\omega\right]^2 + \left[\alpha\left(\frac{c}{\mu}\right)^2 - (\cos\omega)^2\left(\sigma_t + \sigma_\varepsilon\left[\frac{\sigma_\varepsilon^2}{\mu^2\sigma_t^2}\right]\right)\right]\sigma_t}}{\alpha(\cos\omega/\mu)^2 - (\sin\omega)^2}
\end{aligned} \tag{7}$$

Where μ and σ_ε are, the slope and the intersection of the hyperbola, respectively. Also, $\sigma_1(\omega)$, asymptote with the σ_N axis. σ_t, σ_c and σ_s are the mesoscale tensile, compressive and shear strength, respectively. The term σ_0 corresponds to the intersection of the curves $\sigma_1(\omega)$ and $\sigma_2(\omega)$.

The form below is used for $K(\omega)$:

$$K(\omega) = \begin{cases} K_c\left[1 - \left(\dfrac{\omega + \pi/2}{\omega_0 + \pi/2}\right)^{nc}\right] & \omega \le \omega_0 \\ K_t\left(\dfrac{2\omega}{\pi}\right)^{nt} & 0 < \omega \le \dfrac{\pi}{2} \\ 0 & \omega_0 \le \omega \le 0 \end{cases} \tag{8}$$

Parameters K_c and n_c control the nonlinear compressive and low shear-high compressive response and k_t and n_t govern the nonlinear tensile, shear-tensile and high shear-low compressive behavior at meso-level.

Calibration and Validation

Preliminaries: In order to realistically simulate a specific concrete in the LDPM, one is supposed to determine the basic parameters of the model in such a way that the final responses of the numerical models match the corresponding experimental results. It needs to be noted that for a successful calibration process, one should know how the macroscopic responses of the concrete are connected to the meso-scale parameters of the LDPM. In this study, the calibration procedure proposed by Mencarelli [25] has been combined with our experience with the LDPM and a simple reliable calibration procedure is extracted. It requires the results of the three tests of uniaxial compression, uniaxial tension and hydrostatic compression. In the following sections, the experimental results of Barbosa et al. [3] are used to calibrate the model. Next, the model is validated in the case of a hollow concrete block made of the very same concrete.

Calibration: In the first calibration step, α and E_N are determined by matching the elastic responses of an unconfined uniaxial compression simulation with those of the experiment. It is important to note that, as the friction coefficient between the loading plates and the specimens is not reported [3], this parameter is reasonably assumed

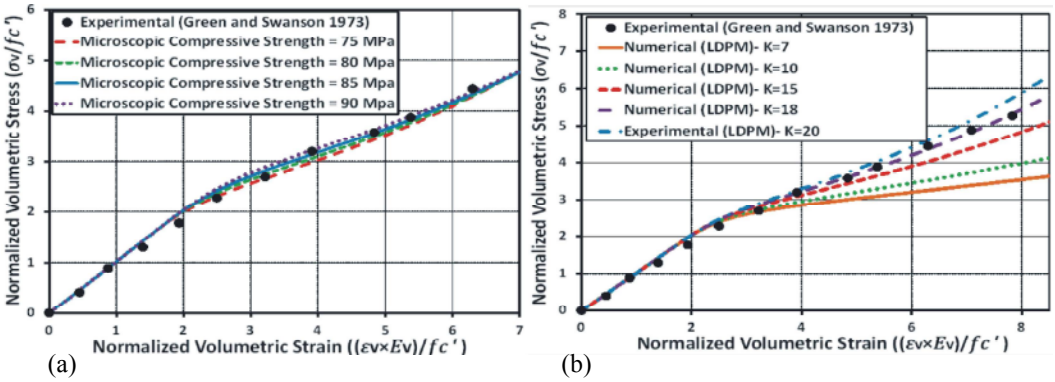

Fig. 2: Estimating parameters from the normalized hydrostatic curve. (a) σ_c *and (b)* K_c

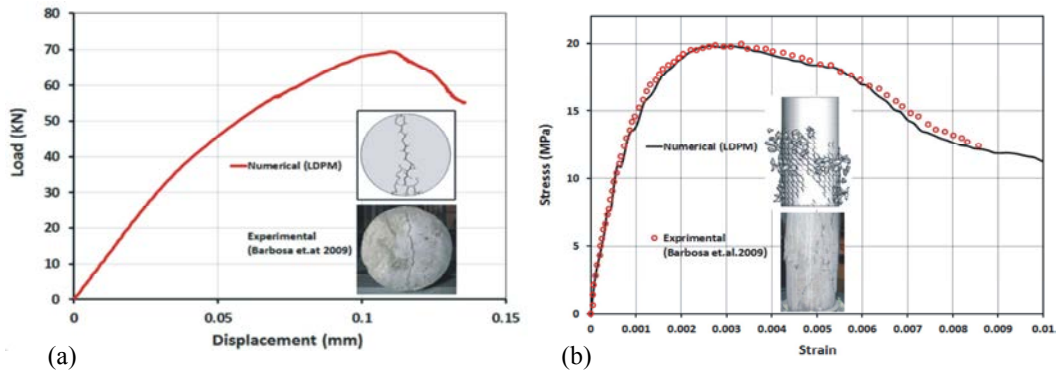

Fig. 3: Response of the cylindrical specimen under. (a)Indirect tension and (b) uniaxial compression.

equal to 0.1. The only parameter affecting the Poisson's ratio of the model is α, thus its accurate value can simply be estimated. Furthermore, the identification of E_N requires that the initial elastic slope of the stress-strain curve coincide with its experimental counterpart. At the end of this stage we have the correct values of α and E_N. They will be considered fixed parameters during the remaining steps of calibration.

The next stage is to identify σ_c and K_c. It is found by Mencarelli [25] that these parameters decide the location of slope change on the normalized hydrostatic compression curve and its initial inelastic slope, respectively. In the absence of appropriate experimental data, Mencarelli [25] has suggested to use available information from other experimental work, generally driven out for the hydrostatic compressive behavior of concrete material [27]. Figs. 2a and 2b illustrate how these two parameters are estimated in a trial and error procedure.

Next, the tensile strength of meso-structure, (σ_t), should be found in a way that the tensile strength of the model matches the experimental value (Fig. 3a). Here, an indirect tensile test (splitting test) is performed and the tensile strength is obtained by comparing the peak values of the force-displacement curves. In the last step n_t and σ_s are acquired through a trial and error process with the aim of reaching the correct peak value and post peak slope of the uniaxial compressive curve.

Fig. 3b shows a comparison between the numerical and experimental results of the uniaxial compression test. It should be noted that the tensile and compression tests were performed on standard 100×200 mm cylindrical specimens. The numerical models also correctly predict crack patterns of the cylindrical specimens. A diagonal mode of cracking in addition to a slight crushing at the middle of the height of the compressive concrete cylinder is observed which is the same as the cracks formed in the experimental test (Fig. 3b) [28]. Also, for both tensile samples, a similar vertical crack is recorded which is due to the direct loading conditions at the top and bottom of the horizontal cylindrical specimen (Fig. 3a). At this stage, all the required parameters to model a desired type of concrete are drawn out which will all be used as inputs for the validation and further numerical analysis. Table 1 presents concrete meso-scale parameters together with their definitions and calibrated values. Table 2 compares the numerically and empirically obtained properties of the concrete.

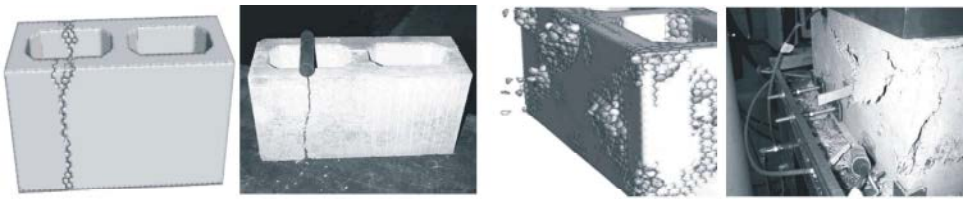

(a) (b) © (d)

Fig. 4: Failure mechanism of the hollow block. (a) Indirect tension (LDPM), (b) indirect tension (experiment), (c) uniaxial compression (LDPM), and (d) uniaxial compression (experiment).

Table 1: LDPM calibrated parameters

Parameter	Definition	Calibrated Value
α	Parameter controlling the Poisson's ratio	0.2
E_N	Normal Young's modulus of the meso-structure	50 (GPa)
K_c	Initial hardening modulus	18
σ	Compressive strength of the meso-structure	85 (MPa)
σ_t	Tensile strength of the meso-structure	3.2 (MPa)
n_t	Parameter describing the behavior of softening slope	1.0
σ_s	Shear strength of the meso-structure	4.8 (MPa)

Table 2: Final Mechanical properties of the concrete

Mechanical properties	Experimental	Numerical (LDPM)
Compressive Strength (MPa)	20	20
Strain at Failure	2707	2700
Modulus of Elasticity (MPa)	19407	19500
Tensile Strength (MPa)	2.2	2.2

Validation: In the validation phase, the experimental results of Barbosa [28] for the compressive and tensile loading of a specific type of hollow concrete block were used. The ultimate forces resisted in the numerical model under compression and indirect tensions were compared with the experimental results. The peak value of the numerical compressive load-displacement curve was equal to 628.41 KN. Dividing this quantity to the cross-sectional area of the block (306 cm^2), the strength value of 20.5 MPa is obtained which is in good agreement with the experimental value of 20.1 MPa. Furthermore, the failure modes of tested specimens were also investigated. Figs. 4a and 4b compare the cracking pattern of the block under indirect tension and Fig. 4.c and 4.d show that for the specimen under compression, both in numerical and experimental tests, respectively. In the indirect tension test, due to the local loading, a vertical crack occurs through the height of the block. However, because of the confinement produced by the loading plates at the top and bottom of block in compression test, diagonal crack with crushing proceeded in the sides of the blocks. Thus the failure mode is a combination of shear and compression failures. As demostrated, the experimental observations are satisfactorily predicted by the LDPM simulations.

Block Analysis: The detailed numerical analysis of the block units under different loading states to which are prominently s ubjected, can lead to a reliable design. The types of loads mostly affecting masonry walls include gravity f orces due to the weight of the walls and other structural elements standing on them, as well as lateral loads caused by earthquake or wind. Here, to have a realistic observation of block responses in masonry buildings, each block is subjected to simultaneous gravity and shear loads and is analyzed using the computer code written based on the Lattice Discrete Particle Model. In each loading step of the LDPM analysis, a vertical displacement in addition to a horizontal displacement is applied to the nodes of the top surface of each block while the bottom nodes of the block are constrained according to the test conditions. In this work, four types of blocks were analyzed under combined action of compression and shear. All the blocks considered in this research were 140×190×390 mm two-core samples. To optimize the blocks behavior, initially a typical form of two-core block is taken. In the second and third blocks, a 30 mm horizontal diaphragm has been inserted in the bottom and middle of the blocks, respectively. An extra fourth sample is also studied in which the holes are rearranged. All four types of blocks have equal cross sectional areas but the weight of each block varies according to its geometrical configuration. Table 3 presents the cross section, longitudinal section and weight of each block.

Table 3: Analysed blocks

	Block type 1	Block type 2	Block type 3	Block type 4
Cross Section				
Longitudinal Section				
Weight (N)	137	154	154	137

RESULTS AND DISCUSSIONS

The simulations are carried out by applying displacement-controlled compression while assuming constant ratios (0, 0.5, 1, 2.5, 5 and 10) of lateral to axial displacements. Considering a 2 mm compressive displacement, shear displacements equal to 0, 1, 2, 5, 10 and 20 are applied to the blocks. Fig. 5a shows the peak compressive load versus the peak shear load resisted by each block. It is obvious that block type 2 with the highest curve and block type 1 with the lowest curve have the best and worst compressive resistance under combined effect of shear and compression, respectively. It can also be concluded from the curves in Fig. 5a that, among block types 3 and 4, the former behaves relatively better for lower shear loads; however, as the share of shear increases, block type 3 proves its superiority.

The above comparisons are merely based on the pure strength; however, the blocks used in any load bearing structure, should have the least possible weight due to structural and handling requirements. Hence, the optimum option should be selected according to simultaneous attention to both the strength and weight. A non-dimensional variable called the optimality index (*OI*), is calculated as introduced below:

$$OI = \frac{P_{peak}}{Weight} \tag{9}$$

The curves of Fig. 5b depicts the optimality index of blocks versus the displacement ratio (shear to compression) applied to each specimen. According to the results, block type 4 which no added diaphragm gives the best response in shear to compression ratios of less than 4. This means that in such loading conditions, the increasing effect of a horizontal diaphragm on the weight is more than that on the strength. For the ratio greater than 4 the responses of the three blocks of types 2, 3 and 4 are similar. Still, block type 1, with its traditional form, owns the worst effective strength in any shear-compression combinations.

In order to have a more precise comparison between the responses of blocks, their failure modes should also be taken into consideration. Observing the exact crack patterns, their directions and the amount of damage caused in the webs, shells or face-shell connections of each block, we will come to a complete conclusion for the strong and weak points. For this purpose, the graphical outputs that show the failure patterns of the analyzed blocks are generated by a post-processing code written for the Lattice Discrete Particle Model. In this code, each aggregate with a specified grout volume surrounding the aggregate is considered as a rigid cell. Each rigid cell is connected to the adjacent rigid cells of the concrete material through connection points (Fig. 6). The average strain in each of these connection points is calculated according to the effective strains of the computational points. Considering the average strains in each connection point, the rotations and displacements of each particle and the final deformed and cracked shape of the concrete specimen are visualized. Fig. 7 shows these graphical results.

As shown, a diagonal crack is observed on the face-shell of all blocks. Block type 1 has more damaged and crushed areas than others, especially on the top surface, which confirm its worst load resistance capacity. The presence of a horizontal diaphragm in block types 2 and 3 prevents continuous crack propagations. Suitable block types may be produced by changing the thickness or shape of the diaphragm inserted. It is interesting that, for block type 4, the presence of two thick internal walls, compared to the three thinner internal walls of other samples, increases the effect of confinement and thus improves its optimality index. Another important advantage of using block type 4, apart from its optimality, is that no additional plate is required in its construction.

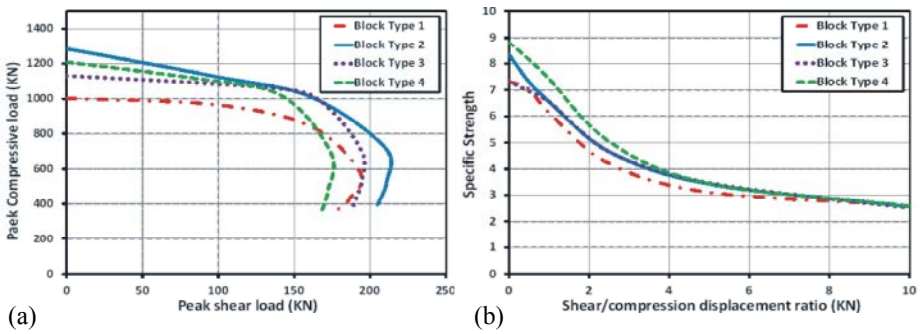

(a) (b)

Fig. 5: Block responses. (a) Peak compressive vs. shear loads and (b) specific strength vs. displacement ratio.

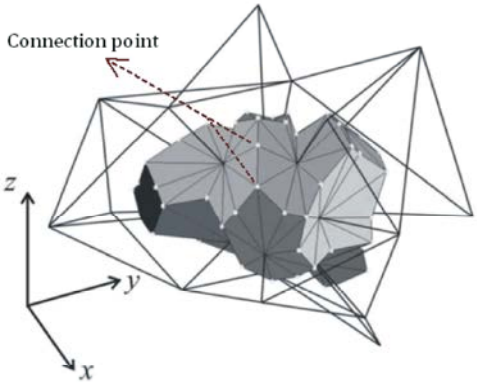

Fig. 6 : Connection points of a Concrete aggregate-mortar cell [24]

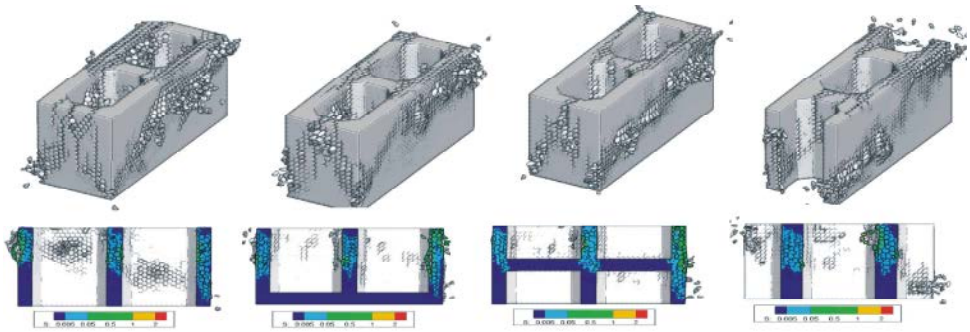

Block type 1 Block type 2 Block type 3 Block type 4

Fig. 7 : Failure modes of the blocks and effective strain contour of their longitudinal sections

CONCLUSION

The application of numerical methods with discrete nature to the meso-scale simulation of concrete as a multi-phase material can help us deepen our understanding of the underlying mechanisms involved in its failure. Inspired by this fact, the newly developed Lattice Discrete Particle Model is incorporated in this research. A homemade graphical code is also utilized to manipulate the outputs of the models.

The LDPM model is calibrated for the available compressive and tensile test results on cylindrical samples so that the required parameters of the model are obtained for the modeling of a specific concrete. In the next part of the paper, results of numerical simulations on a hollow concrete block were validated against the results of an experimental test previously conducted on similar hollow concrete blocks. Next, the response of four two-hole hollow concrete blocks under different combinations of shear and compression were assessed.

It is numerically observed that inserting a horizontal wall in the middle or the bottom of a block can increase its ultimate effective strength (load resistance/weight). Furthermore, it is found that, keeping weight constant, the block having one hole in the middle and two half holes in its both sides behaves better than the block having two complete internal holes. This can be attributed to its more thick internal walls in which the effect of confinement is more pronounced.

REFERENCES

1. Maurenbrecher, A., 1986. Axial compression tests on masonry walls and prisms. In Proc. Third North Am. Mason. Conf. held 3-5 June 1985, University of Texas at Arlington, 1985. pp: 1.
2. Maurenbrecher, A., 1986. Compressive Strength of Hollow Concrete Blockwork.
3. Barbosa, C. and J.B. Hanai, 2009. Strength and deformability of hollow concrete blocks: correlation of block and cylindrical sample test results. IBRACON Structures and Materials Journal. 2(1).
4. Ramamurthy, K., V. Sathish and R. Ambalavanan, 2000. Compressive strength prediction of hollow concrete block masonry prisms. ACI Structural Journal. 97(1).

5. Andolfato, R.P. and J.S. Camacho, 2007. Brazilian results on structural masonry concrete blocks. ACI Materials Journal. 104(1).
6. Page, E.A. and N. Shrive, 1990. Concentrated loads on hollow concrete masonry. ACI Structural Journal. 87(4).
7. Yi, J. and N.G. Shrive, 2003. Behaviour of partially grouted hollow concrete masonry subjected to concentrated loads. Canadian Journal of Civil Engineering. 30(1): 191-202.
8. Grimm, C.T. and R.L. Tucker, 1985. Flexural Strength of Masonry Prisms versus Wall Panels. Journal of Structural Engineering. 111(9): 2021-2032.
9. Drysdale, R.G., W.W. El-Dakhakhni and E.A. Kolodziejski, 2008. Shear capacity for flange-web intersection of concrete block shear walls. Journal of Structural Engineering. 134(6): 947-960.
10. Hamid, A.A. and A.O. Chukwunenye, 1986. Compression behavior of concrete masonry prisms. Journal of Structural Engineering. 112(3): 605-613.
11. Ganesan, T. and K. Ramamurthy, 1992. Behavior of concrete hollow-block masonry prisms under axial compression. Journal of Structural Engineering. 118(7): 1751-1769.
12. Köksal, H.O., C. Karakoc and H. Yildirim, 2005. Compression behavior and failure mechanisms of concrete masonry prisms. Journal of materials in civil Engineering. 17(1): 107-115.
13. Wu, C. and H. Hao, 2008. Numerical derivation of averaged material properties of hollow concrete block masonry. Engineering Structures. 30(3): 870-883.
14. Barbosa, C.S., P.B. Lourenço and J.B. Hanai, 2010. On the compressive strength prediction for concrete masonry prisms. Materials and structures 43(3): 331-344.
15. Lu, M., A.E. Schultz and H.K. Stolarski, 2011. Influence of cavity dimension on the stability of eccentrically loaded slender unreinforced masonry hollow walls. Construction and Building Materials 25(12): 4444-4453.
16. Anand, K. and K. Ramamurthy, 2000. Development and performance evaluation of interlocking-block masonry. Journal of Architectural Engineering. 6(2): 45-51.
17. Thanoon, W.A., M.S. Jaafar, M.R. Abdul Kadir, A.A. Abang Ali, D. Trikha and A. Najm, 2004. Development of an innovative interlocking load bearing hollow block system in Malaysia. Construction and Building Materials. 18(6): 445-454.
18. Jaafar, M.S., W.A. Thanoon, A. Najm, M.R. Abdulkadir and A.A. Abang Ali, 2006. Strength correlation between individual block, prism and basic wall panel for load bearing interlocking mortarless hollow block masonry. Construction and Building Materials. 20(7): 492-498.
19. Thanoon, W.A.M., A.H. Alwathaf, J. Noorzaei, M.S. Jaafar and M.R. Abdulkadir, 2008. Finite element analysis of interlocking mortarless hollow block masonry prism. Computers & Structures. 86(6): 520-528.
20. Del Coz Díaz, J., P.J. García Nieto, F.P. Álvarez Rabanal and A. Lozano Martínez-Luengas, 2011. Design and shape optimization of a new type of hollow concrete masonry block using the finite element method. Engineering Structures. 33(1): 1-9.
21. Cusatis, G., 2001. Tridimentional random particle model for concrete, Politecnico di Milano. PhD thesis.
22. Cusatis, G., Z.P. Bazant and L. Cedolin, 2003. Confinement-shear lattice model for concrete damage in tension and compression: I. theory. Journal of Engineering Mechanics. 129(12): 1439-1448.
23. Cusatis, G., Z.P. Bazant and L. Cedolin, 2003. Confinement-shear lattice model for concrete damage in tension and compression: II. Computation and validation. Journal of Engineering Mechanics. 129(12): 1449-1458.
24. Cusatis, G., Z.P. Ba_ant and L. Cedolin, 2006. Confinement-shear lattice CSL model for fracture propagation in concrete. Computer Methods in Applied Mechanics and Engineering. 195(52): 7154-7171.
25. Mencarelli, A., 2007. The Lattice Discrete Particle Model (LDPM) for Concrete: Calibration and Validation under Quasi-Static Loading Conditions. M.Sc Thesis. Rensselaer Polytechnic Institute Troy, New York.
26. Mencarelli, A., 2010. Numerical Simulation of the Effect of Blast and Penetration on Reinforced Concrete Structures.
27. Green, S. and S. Swanson, 1973. Static constitutive relations for concrete. DTIC Document.
28. Barbosa, C.S., 2004. Resistência e deformabilidade de blocos vazados de concreto e suas correlações com as propriedades mecânicas do material. constituinte MSc thesis. Universidade de Sao Paulo.